

Excitons and excitonic fine structures in Si nanowires: Prediction of an electronic state crossover with diameter changes

Lijun Zhang, Jun-Wei Luo, Alberto Franceschetti, and Alexander Zunger*

Lijun Zhang, Jun-Wei Luo, Alberto Franceschetti, and Alexander Zunger
 (Received 12 April 2011; published 1 August 2011)

Si nanowires have attracted considerable attention as promising candidates for electronic, thermoelectric, photonic, and photovoltaic devices, yet there appears to be only limited understanding of the underlying electronic and excitonic structures on all pertinent energy scales. Using atomistic pseudopotential calculations of single-particle as well as many-body states, we have identified remarkable properties of Si nanowires in three energy scales: (i) In the high-energy ~ 1 -eV scale, we find an unusual electronic state crossover where the nature of the lowest occupied molecular orbital (LUMO) state changes its symmetry with wire diameters for [001]-oriented wires but not for [011]-oriented wires. This change leads to orbitally allowed transitions becoming orbitally forbidden below a certain critical diameter for [001] wires. (ii) In the intermediate-energy $\sim 10^{-1}$ -eV scale, we describe the details of the electron-hole exchange interaction, whereas the spin-allowed states in the orbitally forbidden diameter region remain dark. The diameter dependence of the fine-structure splitting of excitonic states scales as $1/D$

2.3

in [001] wires and as $1/D^{2.6}$ in [011] wires. Surface-polarization effects are found to significantly enhance electron-hole Coulomb interaction, but have a small effect on the exchange fine-structure splitting. The present work provides a road map for a variety of electronic and optical effects in Si nanowires that can guide spectroscopic studies.

DOI: [10.1103/PhysRevB.84.075404](https://doi.org/10.1103/PhysRevB.84.075404)

PACS number(s): 78.67.Lt, 73.21.Hb, 71.35.Cc, 78.20.Bh

I. INTRODUCTION

Si nanowires have attracted considerable interest as promising candidate structures for electronic,^{1,2} thermoelectric,^{3,4} photonic,^{5,6} and photovoltaic devices,^{7–11} reflected by numerous papers on growth,^{12–14} structural characterization,¹⁵ transport,^{16,17} and optical^{15,18–23} properties. Yet, there appears to be limited understanding of the underlying electronic and excitonic properties. Such understanding should span three energy scales: (i) in the high-energy ~ 1 -eV scale one needs to understand the nature of conduction energy levels and their dependence on wire orientation and diameter (single-particle

here $\mathbf{M} = \sum_{h_i, e_j} C^{(j)}(h_i, e_j) |h_i\rangle \langle e_j| \hat{\mathbf{P}}$ is the dipole transition matrix, E is the exciton energy and the broadening of spectral lines, Γ is chosen as $50 \mu\text{eV}$. The exciton decay lifetime (τ) is calculated according to³⁹

$$\frac{1}{\tau} = \frac{4 E n |\mathbf{M}|^2}{m_0^2 \hbar c^2}, \quad (7)$$

here n is the refractive index (≈ 4.0 for photon

TABLE I. Direct product of interband dipole matrix elements $\langle h|\mathbf{P}_j|e\rangle$ in Si [001] wires (D_{2d} symmetry) and [011] wires (C_{2v} symmetry). \mathbf{P}_j represents the dipole operator along the wire axis (P_{001} for [001] wires and P_{011} for [011] wires) and in-plane direction (P_{110} for [001] and P_{100} for [011]). The symmetric A_1 representation (dipole-allowed transition) is given in bold. For [001] wires the LUMO A_1 is allowed in P_{001} and E is allowed in P_{110} . For [011] wires A_1 is allowed in P_{011} .

[001]:	$\langle h P_{001}(B_2) e\rangle$	$\langle h P_{110}(E) e\rangle$
	B_2 B_2 $A_1 = \mathbf{A}_1$	B_2 E $A_1 = E$
	B_2 B_2 $B_1 = B_1$	B_2 E $B_1 = E$
	B_2 B_2 $E = E$	B_2 E $E =$
		\mathbf{A}_1 A_2 B_1 B_2
[011]:	$\langle h P_{011}(B_1) e\rangle$	$\langle h P_{100}(A_1) e\rangle$
	B_1 B_1 $A_1 = \mathbf{A}_1$	B_1 A_1 $A_1 = B_1$

representations of the D_{2d} group ($|e\rangle = A_1; B_1; E$ and $|h\rangle = B_2$). The dipole operator \mathbf{P}_j consists of two components: P_{001}

corresponds to the electrostatic potential including the surface-polarization effect, and is the solution of the Poisson equation,

$$\nabla^2 \phi(\mathbf{r}) = -4\pi e^2 \sum_j \rho_j(\mathbf{r}). \quad (11)$$

Equations (10) and (11) are solved in real space by using a finite-difference discretization of the gradient operator and a conjugate-gradient minimization algorithm.^{42,43}

In the following we first present results for [001] wires from the above (i), (ii), and (iii) energy scales, and then show results for [011] wires. We then discuss the effects of dielectric mismatch on electron binding and exchange interaction.

A. The eV energy scale: Single-particle states

Bulk Si has six equivalent conduction-band valleys χ (along the $-X$ direction), from which the LUMO of wires is derived. The confinement plane of [001] wires contains four of these six valleys, folded to the Γ point of the wire Brillouin zone. For [001] wires belonging to the D_{2d} point group, symmetry analysis⁴⁴ indicates that these four χ -derived states correspond to the A_1 , B_1 , and E representation, where both A_1 and B_1 are nondegenerate and E is doubly degenerate. The highest occupied molecular orbital (HOMO) always has nondegenerate B_2 symmetry for all wire sizes. Figures 1(a) and 2 show evolution of the LUMO and HOMO state when the wire diameter is varied. At large diameter $D = 7.6$ nm, as quantum confinement and inter-allele coupling are negligible, the splitting between A_1 , B_1 , and E is tiny, leaving all these states practically degenerate. With decreasing diameters, the enhanced inter-allele coupling lifts the degeneracy of these four states. This makes the B_1 state the lowest-energy one at diameter $D = 3.3$ nm to $D = 2.5$ nm (see Fig. 2). For larger diameters, the A_1 state becomes the LUMO [e.g., $D = 2.2$ nm in Fig. 1(a)]. In contrast to the LUMO, the HOMO keeps the B_2 symmetry for all the diameters. These HOMO and LUMO states have characteristic reflections corresponding to their specific symmetries, as shown in the right part of Fig. 1.

The splitting of symmetry of the LUMO state with diameter has a strong effect on the optical properties of these wires. Table I shows the direct product $\langle h|\mathbf{P}_j|e\rangle$ for electron-hole dipole transition matrix elements, in terms of the irreducible

TABLE II. Symmetry analysis of the excitonic states generated from HOMO and LUMO single-particle orbitals of [001] and [011] Si wires. Single-group representations are converted to corresponding double-group representations to include the spin degree of freedom for excitons.

	HOMO	LUMO	Excitons (HOMO × LUMO)
[001]:			
$D = 7.6$ nm	$B_2 - 6$	$E - 6 + 6$	$6 \times 6 = A_1 \ A_2 \ E$
$D = 3.3$ nm	$B_2 - 6$	$B_1 - 6$	$6 \times 6 = A_1 \ A_2 \ E$
$D = 2.2$ nm	$B_2 - 6$	$A_1 - 7$	$6 \times 7 = B_1 \ B_2 \ E$
[011]:			
$D = 3.3$ nm	$B_1 - 5$	$A_1 - 5$	$5 \times 5 = A_1 \ A_2 \ B_1 \ B_2$

B. Intermediate energy scale: Excitonic states

Based on the group theory Table II describes how single-particle HOMO and LUMO states contribute to produce excitons. Here we convert single-group representations to corresponding double-group ones adding the spin degrees of freedom. It can be seen that three groups of excitonic states emerge from different symmetry of the LUMO state:

(1) At diameter $D = 7.6$ nm [Fig. 3(a)], the spin-orbit interaction splits the doubly degenerate LUMO E to $6 + 6$, and also transforms the HOMO B_2 to 6 . This 6×6 manifold in principle should lead to two combinations of $A_1 \ A_2 \ E$ excitonic states, of which the doubly degenerate E state is bright and in-plane polarized. However, due to the weak splitting of the two 6 states (as a result of weak

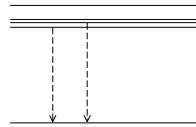
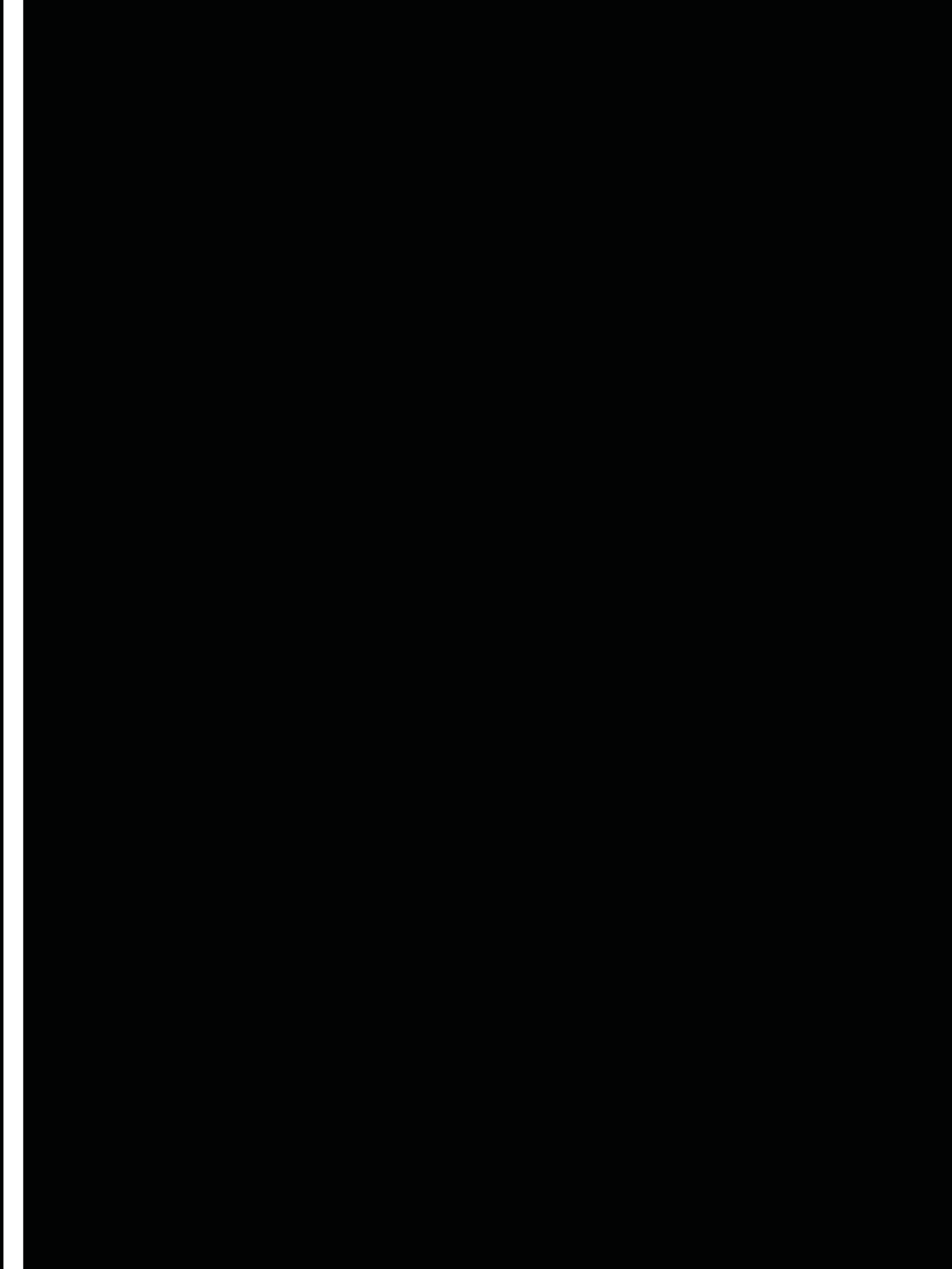


TABLE III. Calculated ground-state exciton energy $E(i)$ and exciton energy level splittings for [001] wires (Fig. 3) and [011] wires (Fig. 6). $E(i)$ ($i = 1, 2, 3$, and 4) represent the energy of excitonic transition corresponding to the notation (1, 2, 3, and 4) in Figs. 3 and 6.

D (nm)	7.6	[001]: 3.3	2.2	[011]: 3.3
$E(1)$ (eV)	1.182	1.460	1.764	1.335
$E(2)-E(1)$ (μeV)	21.3	238.9	399.4	3.4
$E(3)-E(2)$ (μeV)	25.1	721.3	2668.6	20.8
$E(4)-E(3)$ (μeV)	92.4			1017.6

SO coupling), there is strong configuration mixing between these two



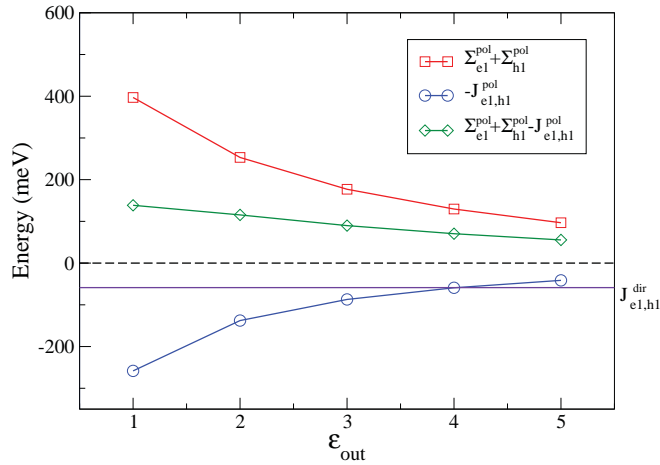


FIG. 8. (Color online) The surface-polarization-induced self-energy ϵ_i^{pol} [$i = e1$ (LUMO) and $h1$ (HOMO)], Coulomb interaction $-J_{e1,h1}^{pol}$ (negative value means decreasing electron energies), and the sum $\epsilon_{e1}^{pol} + \epsilon_{h1}^{pol} - J_{e1,h1}^{pol}$ are shown as a function of ϵ_{out} for a [001] wire of diameter $D = 3.3$ nm. The direct Coulomb interaction (excluding surface-polarization effect) $J_{e1,h1}^{dir}$ is shown as a solid (horizontal) line for comparison.

$\epsilon_{in} = 11.85$ (Ref. 40) for the Si wire and $\epsilon_{out} = 1.5$ for the surrounding material. The calculations are performed for the [001] wire with diameter $D = 3.3$ nm. Fig re 72oe2R(Tj/F51Tf1.0580TD(e)Tj/F11Tf.46370TD[(1)-163.5(())T

